Toward modeling rocket nozzles through artificial boundary conditions

By K. Maeda

1. Motivation and objectives

De Laval (converging-diverging) nozzles are essential components of aerospace chemical propulsion engines for pressurizing a combustion chamber as well as for generating thrusts. In computational fluid dynamics simulations, modeling the nozzle geometry often requires body-fitted grids or immersed boundary techniques. Although high-performance simulations are becoming increasingly capable of accommodating detailed geometries, implementation of such tailored techniques can be cumbersome and may exacerbate the parallel efficiency of a solver when heterogeneous grids are used.

One way to avoid such complexities may be by using an artificial boundary condition (ABC), in which one includes in a numerical domain only a combustion chamber with a uniform cross section without including a nozzle and models the effect of the nozzle through the flux at the domain boundary facing the nozzle (Figure 1). Originally, ABC was developed for accurate simulation of hyperbolic partial differential equations in an unbounded field using a finite-size domain (Engquist & Majda 1977). An ABC is designed to correctly model the transmission of waves at artificial domain boundaries with available information available about the field. Failiure of this process can result in spurious (non-physical) generation of waves which propagate from the boundary into the domain to contaminate the solutions of interest.

A major use of ABCs in fluid dynamics has been in simulation of high-speed flows. The Euler- and Navier-Stokes equations that model the compressible flows are hyperbolic systems, and the characteristic waves in these systems correspond to advection, and acoustic- and shock waves. With a primary requirement for resolving the detailed flow field around the system of interest, such as aero-engines and wings, with limited computational resources, one is often required to limit the domain to include only the near field and exclude the far-field, which may include solutions such as wakes, jets, and radiated sound waves. Much effort has been devoted to the construction of ABCs for both linearized- and nonlinear equations, locally and non-locally, such that spurious reflections of the far-field solutions are mitigated (Colonius 2004). Two major local approaches are the characteristic boundary condition (CBC) and the buffer layer. The former physically models characteristic waves that travel into the domain at its boundary (e.g., Thompson 1987, 1990; Giles 1990; Poinsot & Lele 1992; Colonius *et al.* 1993), while the latter aims to numerically damp undesired reflections through techniques including grid stretching and absorption (e.g., Freund 1997; Hagstrom 1999; Mani 2012).

In this study, we employ a local, approximate, characteristic-based ABC to model the effect of the downstream nozzle on unsteady flow solutions in the domain, namely Nozzle–BC, with a primary interest in future applications to the simulation of complex flows in real rocket engines. The approach essentially extends the time–dependent boundary condition for compressible sub-sonic flows exiting a domain boundary (Thompson 1990; Poinsot & Lele 1992). In Nozzle–BC, we assume quasi–static response of the flow in

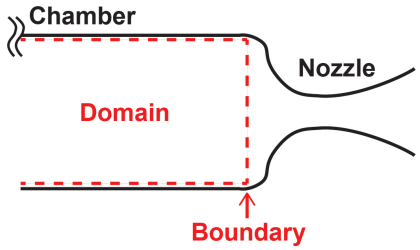

FIGURE 1. Schematic of the problem.

the nozzle to the unsteady variation of the flow state at the nozzle inlet, in that the flow inside the nozzle instantly adjusts to the one-dimensional (1D) solution following isentropic nozzle flow equations. This assumption enables us to relate the flow state at the domain boundary to that at the outlet or the throat of the nozzle, where constraints are applied by the equations. When the nozzle is unchoked, we force the characteristic wave traveling into the domain such that the pressure at the nozzle outlet is maintained at the back-pressure. When the nozzle is choked, we force both incoming and outgoing characteristic waves such that the Mach number of the flow at the nozzle throat is frozen at unity and the pressure at the nozzle inlet is simultaneously adjusted.

The rest of the brief is organized as follows. In Section 2, we formulate Nozzle–BC using the characteristic form of the Euler equation. In Section 3, we demonstrate the method through simulation of the unsteady pressurization of a combustor attached to a converging nozzle. Solutions obtained using Nozzle–BC with the domain excluding the nozzle are compared with those obtained using the standard CBC and the nozzle included in the domain. A quasi–1D solver is used for these simulations. In Section 4, we state conclusions and present an outlook for future work.

2. Methods

2.1. *Characteristic equation*

We formulate the dynamics of a compressible fluid using the Euler equation as

$$\frac{\partial \boldsymbol{U}}{\partial t} = \frac{\partial \boldsymbol{F}}{\partial \boldsymbol{x}}, \tag{2.1}$$

where $\boldsymbol{U}$ and $\boldsymbol{F}$ are the conserved variables and the flux,

$$\boldsymbol{U} = [\rho, \rho \boldsymbol{u}, E]^T, \tag{2.2}$$

$$\boldsymbol{F} = [\rho \boldsymbol{u}, \rho \boldsymbol{u}^2 + p, (E + p)\boldsymbol{u}]^T. \tag{2.3}$$

For simplicity we omit viscosity, heat transfer, chemical reaction, and body force. One could readily extend the present analysis to include them.

We re-write this equation on x_1-x_2-x_3 Cartesian coordinates as

$$\frac{\partial \boldsymbol{U}}{\partial t} = \boldsymbol{A_1}\frac{\partial \boldsymbol{U}}{\partial x_1} + \boldsymbol{A_2}\frac{\partial \boldsymbol{U}}{\partial x_2} + \boldsymbol{A_3}\frac{\partial \boldsymbol{U}}{\partial x_3}, \tag{2.4}$$

where $\boldsymbol{A}_i$ is the flux Jacobian in the x_i direction: $\boldsymbol{A}_i = \partial \boldsymbol{F}/\partial \boldsymbol{U}|_{x_m (m \neq i)}$.

In this study, we assume that the boundary of interest is perpendicular to the x_1 axis with its exterior pointing in the positive x_1 direction, and omit without loss of generality

the terms associated with the flux in the x_2 and x_3 directions from the equation as

$$\frac{\partial \boldsymbol{U}}{\partial t} = \boldsymbol{A_1}\frac{\partial \boldsymbol{U}}{\partial x_1}. \tag{2.5}$$

By considering characteristic decomposition of $\boldsymbol{A}_1$: $\boldsymbol{A}_1 = \boldsymbol{S\Lambda S}^{-1}$ and multiplying $\boldsymbol{S}^{-1}$ from the left of the equation, we obtain the characteristic equation

$$\boldsymbol{S^{-1}}\frac{\partial \boldsymbol{U}}{\partial t} = \boldsymbol{\Lambda S^{-1}}\frac{\partial \boldsymbol{U}}{\partial \boldsymbol{x}}. \tag{2.6}$$

For convenience, following Thompson (1987, 1990) and Poinsot & Lele (1992), we express this equation component-wise as

$$\boldsymbol{l_i^T}\frac{\partial \boldsymbol{U}}{\partial t} + L_i = 0, \tag{2.7}$$

where $\boldsymbol{l}_i$ is the left eigenvector of $\boldsymbol{A}$ and

$$L_i = \lambda_i \boldsymbol{l}_i^T \frac{\partial \boldsymbol{U}}{\partial \boldsymbol{x}}. \tag{2.8}$$

λ_i are the eigenvalues of A obtained as

$$\lambda_1 = u_1 - c, \qquad \lambda_2 = \lambda_3 = \lambda_4 = c, \qquad \lambda_5 = u_1 + c, \tag{2.9}$$

where c is the sound speed. L_i represents the characteristic wave propagating at a speed of λ_i perpendicular to the domain boundary, and the direction of the wave is dependent on the local Mach number. For instance, for supersonic out-flows, $\lambda_i > 0$ for all the waves and they travel out from the domain, while for subsonic out-flows $\lambda_1 < 0$ and the corresponding wave propagates into the domain from the exterior to alter the solution in the domain. The spirit of the CBC is to physically model the incoming wave, combining information about the interior with information about the exterior. In the present study, the flow in the combustor is subsonic and directed outward to the nozzle, and $\lambda_1 < 0$ and $\lambda_{2-5} > 0$. We therefore expect to primarily model the incoming wave corresponding to L_1.

Now we express Eq. (2.7) in terms of primitive variables for ideal gas as follows.

$$\frac{\partial \rho}{\partial t} + \frac{1}{c^2}\left[L_2 + \frac{1}{2}(L_5 + L_1)\right] + u_2\frac{\partial \rho}{\partial x_2} + u_3\frac{\partial \rho}{\partial x_3} + \rho\left(\frac{\partial u_2}{\partial x_2} + \frac{\partial u_3}{\partial x_3}\right) = 0, \tag{2.10}$$

$$\frac{\partial p}{\partial t} + \frac{1}{2}(L_5 + L_1) + u_2\frac{\partial p}{\partial x_2} + u_3\frac{\partial p}{\partial x_3} + \gamma p\left(\frac{\partial u_2}{\partial x_2} + \frac{\partial u_3}{\partial x_3}\right) = 0, \tag{2.11}$$

$$\frac{\partial u_1}{\partial t} + \frac{1}{2\rho c}(L_5 - L_1) + u_2\frac{\partial u_1}{\partial x_2} + u_3\frac{\partial u_1}{\partial x_3} = 0, \tag{2.12}$$

$$\frac{\partial u_2}{\partial t} + L_3 + u_2\frac{\partial u_2}{\partial x_2} + u_3\frac{\partial u_2}{\partial x_3} + \frac{1}{\rho}\frac{\partial p}{\partial x_2} = 0, \tag{2.13}$$

$$\frac{\partial u_3}{\partial t} + L_4 + u_2\frac{\partial u_3}{\partial x_2} + u_3\frac{\partial u_3}{\partial x_3} + \frac{1}{\rho}\frac{\partial p}{\partial x_3} = 0, \tag{2.14}$$

where γ is the specific heat ratio. For simplicity, we consider flows uniform on the exit boundary tangential to the x_2 and x_3 axes. The set of equations can then be simplified

as

$$\frac{\partial \rho}{\partial t} + \frac{1}{c^2}\left[L_2 + \frac{1}{2}(L_5 + L_1)\right] = 0, \tag{2.15}$$

$$\frac{\partial p}{\partial t} + \frac{1}{2}(L_5 + L_1) = 0, \tag{2.16}$$

$$\frac{\partial u_1}{\partial t} + \frac{1}{2\rho c}(L_5 - L_1) = 0. \tag{2.17}$$

In the following sections, we use this simplified set of equations to construct Nozzle–BC to prove its concept. The question to be answered is how to define L_1, L_2, and L_5 at the domain boundary (nozzle inlet) such that the physical constraint introduced by the nozzle is satisfied.

2.2. *Nozzle flow equations*

The theory of gas dynamics in converging-diverging nozzles is widely used and available elsewhere (e.g., Anderson 2003). For simplicity, we neglect viscosity of the gas and heat transfer across the nozzle wall. The geometry of the nozzle is characterized by the inlet area A_i, throat area, A^*, and exit area, A_e. With the given geometry, the flow state in the isentropic nozzle flow is uniquely characterized by the stagnation (reservoir) pressure of the flow, p_0, and the back-pressure, p_b. The following equations relate the isentropic flow in the nozzle and the stagnation state.

$$p = f_p(p_0, M) = p_0 \left(1 + \frac{\gamma - 1}{2} M^2\right)^{-\frac{\gamma}{\gamma - 1}}, \tag{2.18}$$

$$\dot{m} = f_m(A, M, p_0, \rho_0) = \sqrt{\rho_0 p_0} A M \left(1 + \frac{\gamma - 1}{2} M^2\right)^{-\frac{\gamma + 1}{-2(\gamma - 1)}}, \tag{2.19}$$

where $\dot{m}$ is the mass flow rate, A and M are the cross–sectional area and the Mach number of the flow in the nozzle, and ρ_0 is the stagnation density.

The flow in the nozzle following these relations takes two distinct regimes, the so-called unchoked- and choked regimes, depending on the pressure ratio, p_b/p_0. With a fixed p_b (which is typically ambient) and increasing p_0, the Mach number of the flow at the throat, M_t, increases. There exists a critical stagnation pressure p^* at which M_t reaches unity. When $p_0 < p^*$, the flow is unchoked. The flow remains subsonic throughout the nozzle, and the pressure at the nozzle outlet corresponds to p_b. In this regime, the flow is accelerated in the converging section and decelerated in the diverging section. In contrast, the flow is choked at $p_0 > p^*$. In this regime, M_t remains at unity regardless of p_0. The flow remains supersonic after passing the throat and can be accelerated to increase its Mach number in the diverging section. This acceleration generates the thrust. In both regimes, the pressure at the nozzle inlet is greater than the back-pressure when $A_i > A_e$.

From the perspective of the CBC, the two regimes have a critical difference. In the unchoked regime, the flow is sub-sonic and information in the nozzle exterior propagates into the combustor through the nozzle. In the choked regime, since the flow becomes sonic at the throat, information downstream of the throat does not propagate back into the domain. To construct Nozzle–BC, we therefore use distinct procedures to model the two regimes.

2.3. *Nozzle–BC for unchoked flow*

To construct Nozzle–BC in the unchoked regime, we assume that the flow in the nozzle quasi–staticaly changes with the state of the inlet. This assumption is valid when the length scale of the unsteady disturbance of the flow is smaller than the length of the nozzle. Qualitatively speaking, we aim to alter L_1 based on the constraint that the pressure at the nozzle exit, p_e, is maintained at p_b. The procedure of the modeling is as follows.

(1) Compute the stagnation pressure, p_0, from p_i and M_i: $p_i = f_p(p_0, M_i)$.
(2) Given this value of p_0, compute the Mach number of the flow at the nozzle outlet, M_e, by solving the following relation.

$$f_m(A_i, M_i, p_0, \rho_0) = f_m(A_e, M_e, p_0, \rho_0). \tag{2.20}$$

(3) Obtain p_e from M_e and p_0: $p_e = f_p(p_0, M_e)$.
(4) Penalize L_1 with the offset of p_e from p_b: $L_1 = K(p_e - p_b)$, where K is a constant with a unit of s^{-1}.

This penalization is similar to standard CBCs for subsonic outflow that is designed to maintain a constant pressure at a domain boundary considered by Rudy & Strikwerda (1980) and Poinsot & Lele (1992). Following these studies, K can be defined as $K = C(1-M^2)c/L_d$, where M is the maximum Mach number in the flow, L_d is the characteristic length of the domain, and C is a constant. Without penalization, $L_1 = 0$. The incoming wave is modeled as zero and the boundary condition becomes essentially non-reflective (i.e., non-reflective characteristic boundary condition, NRCBC).

2.4. *Nozzle–BC for choked flow*

The construction of Nozzle–BC in the choked regime requires a modification to the unchoked case. The physical constraint in the choked regime is $M_t = 1$ at the nozzle throat. With the quasi–equilibrium assumption, this constraint can be translated through Eq. (2.19) such that the Mach number is frozen everywhere upstream of the throat, including the inlet. The pressure ratio, p_i/p_0, is likewise frozen (Eq. (2.18)). Therefore, the CBC is required to satisfy these two constraints at the same time. The constraint on the Mach number can be expressed as

$$\frac{\partial M^2}{\partial t} = \frac{\partial}{\partial t}\left(\frac{\rho u^2}{\gamma p}\right) = 0. \tag{2.21}$$

This equation can be rewritten as

$$\frac{u^2}{\rho}\frac{\partial \rho}{\partial t} + \rho u \frac{\partial u}{\partial t} - \frac{M^2}{\gamma}\frac{\partial p}{\partial t} = 0. \tag{2.22}$$

By using Eq. (2.22) as well as Eqs. (2.15-2.17), we can obtain the following relation for L_1, L_2, and L_5.

$$\left(\frac{\gamma-1}{2} - \frac{1}{M}\right)L_5 + \left(\frac{\gamma-1}{2} + \frac{1}{M}\right)L_1 - L_2 = 0. \tag{2.23}$$

We do not consider the state of the flow in the diverging part of the nozzle since no characteristic wave propagates upstream from the downstream of the throat where the flow is supersonic. The procedure of the modeling is as follows.

(1) Compute the frozen Mach number at the inlet, $M_{i,f}$, given the choked condition, by solving the relation

$$f_m(A_i, M_i, p_0, \rho_0) = f_m(A_t, M_t = 1, p_0, \rho_0). \tag{2.24}$$

If the nozzle shape does not change with time, $M_{i,f}$ can be computed once and stored throughout the simulation.

(2) Compute p_0 from p_i and $M_{i,f}$: $p_i = f_m(p_0, M_{i,f})$.

(3) Given these values of p_0 and $M_{i,f}$, compute the frozen inlet pressure, $p_{i,f}$: $p_i = f_m(p_0, M_{i,f})$.

(4) Penalize L_1 with the offset of p_i from $p_{i,f}$: $L_1 = K(p_i - p_{i,f})$.

(5) Obtain L_2 using this L_1 and L_5 computed from Eq. (2.8)

$$L_2 = \left(\frac{\gamma - 1}{2} - \frac{1}{M_{i,f}}\right) L_5 + \left(\frac{\gamma - 1}{2} + \frac{1}{M_{i,f}}\right) L_1. \tag{2.25}$$

Alternatively, L_5 can be derived from L_1 and L_2.

In this procedure, we are altering L_2 (L_5) using the penalized L_1. Therefore, the outgoing characteristic waves are implicitly penalized. This penalization may sound counter-intuitive for sub-sonic outflow, for which the CBC is typically required to model only L_1, since L_2 and L_3 are outgoing and are not supposed to affect the solution in the interior. An interpretation is the following. We are physically constraining the flow by using the information at the nozzle throat where the flow is sonic. The domain boundary can therefore be regarded as being virtually extended to the throat. The outgoing waves at the nozzle inlet remain in the interior of this virtual domain until they reach the throat. The modification of L_2 (L_5) can be interpreted as forcing of the interior of the extended domain.

3. Simulation of combustor pressurization

3.1. *Setup*

To demonstrate Nozzle–BC, we simulate pressurization of a combustion chamber in a modeled combustor system. The system is composed of a reservoir, a chamber, and a diverging nozzle in a quasi–1D domain. The flow in this system is modeled using the Euler equation.

The system mimics a real combustor setup. Figure 1 shows the cross section of the real combustor and the cross–sectional radius of the modeled system. The modeled system is defined by the cross–sectional area on the x-coordinate, $A(x) = \pi r^2(x)$. The cross–sectional area relative to that of the chamber, A_0, is defined as

$$\frac{A(x)}{A_0} = 4Rg(-x, x_i, a) + 4(1 - R)(1 - r_t\phi(x, \sigma_t, \mu_t) - r_n g(x, x_n, a)), \tag{3.1}$$

where g and ϕ are the sigmoid function and the Gaussian function, respectively, expressed as

$$g(x, x_i, a) = \frac{1}{1 + e^{a(x - x_i)}}, \tag{3.2}$$

$$\phi(x, \sigma, \mu) = \frac{1}{\sigma\sqrt{2\pi}} e^{-\frac{1}{2}\left(\frac{x-\mu}{\sigma}\right)^2}. \tag{3.3}$$

We use $R = 0.75$, $x_i = 0.039$ m, $x_n = 0.1693$ m, $a_i = 0.0412$ m^{-1}, $\mu_t = 0.0601$ m,

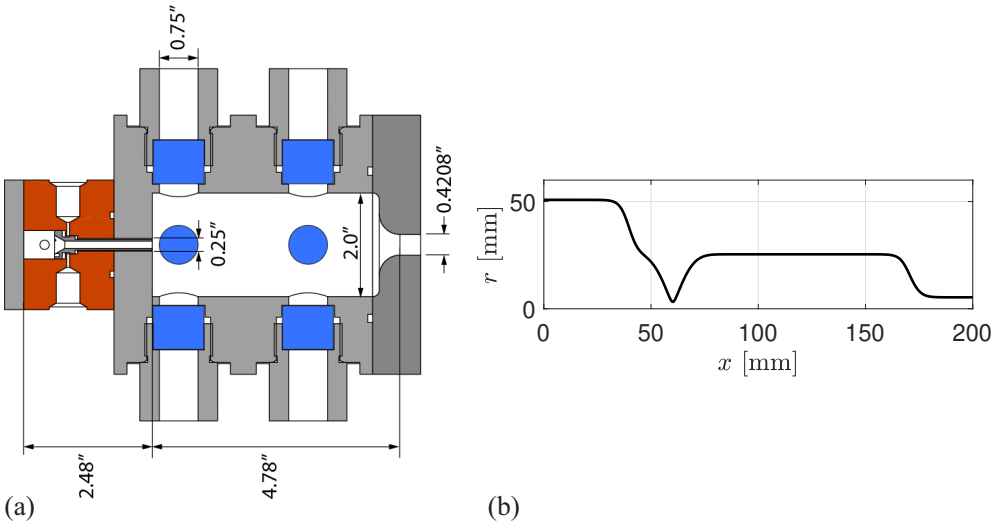

FIGURE 2. (a) Cross section of the gaseous combustor. Units are in inches. (b) Cross–sectional radius of the modeled combustor along the central axis.

$\sigma_t = 0.0064$ m, $r_t = 0.9844$, and $r_n = 0.9559$. The section in $x \in [0, \mu_t]$ corresponds to the injector system in the experiment. In the model, for simplicity this section is treated as a reservoir in which the gas is stagnated. The throat at $x = \mu_t$ corresponds to the chamber inlet at which the gas is introduced at a high speed. The section in $x \in [x_n, 0.2]$ corresponds to the nozzle.

We simulate cases with two distinct setups. In the first setup, the domain is $x \in [0, 0.2]$ m and includes the entire geometry. The outlet boundary condition is initially the subsonic-outflow CBC and is switched to the NRCBC when the flow is choked. This case serves as a reference. In the second setup, the domain is defined as $x \in [0, 0.15]$ m to exclude the nozzle section. Nozzle–BC is used at the right boundary. Various values of K within a range of $K \in [10^4, 10^7]$ are used to assess the effect of the amplitude of the penalization on the solution.

The pressure is initially ambient at 1 bar and uniform in the domain. In all simulation cases, the CBC is used at the left domain boundary. The incoming characteristic wave at the left domain boundary is forced such that the reservoir is rapidly pressurized during the simulation. The treatment of the geometry in the Euler equation follows LeVeque (2002). The domain is discritized with uniform grids with a grid size of $\Delta x = 4.0 \times 10^{-4}$ m. A third-order finite-volume WENO (weighted essentially non-oscillatory) scheme (Jiang & Shu 1996) is used for spatial integration. TVD-RK3 (total variation diminishing third-order Runge-Kutta scheme) (Gottlieb & Shu 1998) is used for time–marching the solution with a sufficiently small time–step size.

3.2. *Results*

Figure 3(a) shows the evolution of the reservoir pressure sampled at the left domain boundary, p_r, and that of the chamber pressure sampled at $x = 0.1$ m, p_c, obtained in simulations using the two setups. For the case using Nozzle–BC, the result with $K = 10^6$ is shown. At around $t = 10$ ms, the reservoir pressure is forced to rapidly grow to 12.5 bar. The evolution of p_r is identical in all simulation cases to the accuracy of interest, regardless of the setup. In both plots, the chamber pressure grows rapidly to around 4

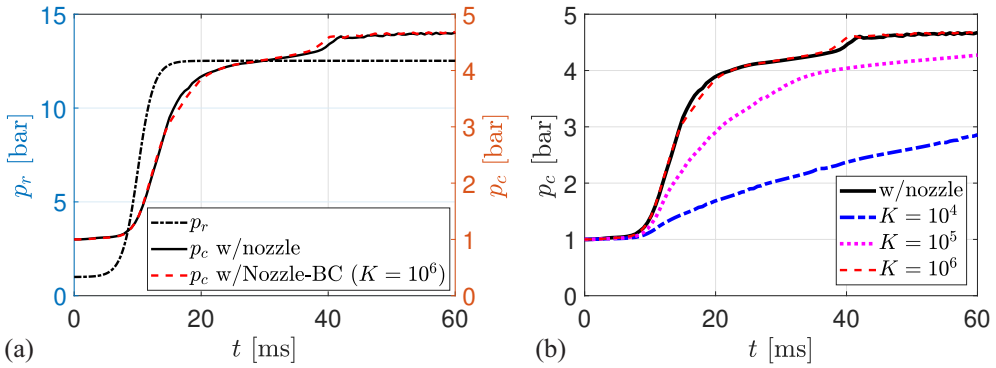

FIGURE 3. (a) Evolution of the reservoir pressure, p_r and that of the chamber pressure, p_c. The reference solution and the solution obtained with Nozzle–BC with $K = 10^6$ are compared. (b) Evolution of p_c obtained with Nozzle–BC with various values of K.

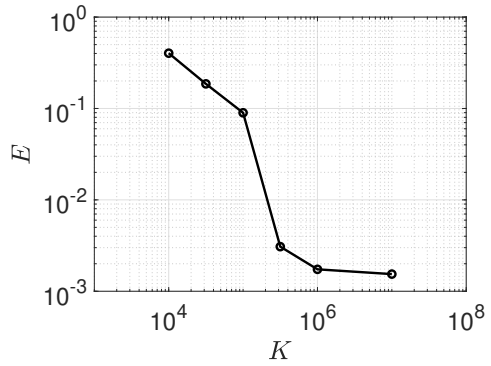

FIGURE 4. Error of the chamber pressure at the steady state computed with Nozzle–BC as a function of K.

bar until $t = 20$ ms and then grows more slowly to reach 4.7 bar at $t = 40$ ms, at which point the solution becomes steady. In both cases, the flow is immediately choked at the chamber inlet after the pressurization of the reservoir begins. The nozzle is choked at $t = 11.6$ ms, at an early stage of the pressurization of the chamber. The two profiles of the chamber pressure agree well with each other. Figure 3(b) compares the plots of the chamber pressure shown in Figure 3(a) and those obtained from the simulation cases with Nozzle–BC with various values of K. The amplitude of the chamber pressure obtained with Nozzle–BC is positively correlated with K throughout the simulation. The pressure profile approaches the reference solution by increasing K from 10^4 to 10^6. The deviation of the profile from the reference solution with small K indicates that the penalization is not sufficient to force the pressure up to the physically desired amplitude.

In order to further quantify the discrepancy of the solution obtained with Nozzle–BC, in Figure 4 we plot the normalized error of the chamber pressure, computed as

$$E = \frac{|\overline{p}_{c,ref} - \overline{p}_c|}{\overline{p}_{c,ref}}, \tag{3.4}$$

where $p_{c,ref}$ is the reference solution and $\overline{(\cdot)}$ denotes the time average over the window of

$t \in [54, 60]$ ms, at which the solution is steady. The plot shows that the error constantly decreases to $O(10^3)$ with increasing K to $O(10^6)$. We do not expect that the error necessarily converges to zero due to the ad hoc nature of the penalization. Nevertheless, the results indicate that Nozzle–BC does a good job of reproducing the reference solution with a sufficiently large, constant value of K.

4. Conclusions

We developed Nozzle–BC, an ABC for simulation of internal compressible flows in a rocket combustor that can be used to model the effect of a downstream nozzle placed outside of a numerical domain. To this end, the CBC for sub–sonic outflows (Thompson 1990; Poinsot & Lele 1992) was extended to account for the constraints imposed by the nozzle flow equations, in both choked and unchoked conditions. We demonstrated the use of Nozzle–BC through quasi–1D simulation of the pressurization of a combustion chamber. Our immediate future work includes comparisons of the simulated pressurization with experimental data. In the meantime, in the simple demonstration presented in this study, we did not consider three-dimensional effects and non-equilibrium dynamics in the nozzle such as unsteady flow separation. Modeling of these and other physical phenomena in Nozzle–BC is part of an ongoing investigation.

Acknowledgments

This investigation was supported by the Department of Energy, National Nuclear Security Administration, under award number DE-NA0003968. The author acknowledges Prof. Sanjiva Lele for valuable discussions and thanks Prof. Carson Slabaugh for providing the schematic of the experimental combustor.

REFERENCES

Anderson, J. D. 2003 *Modern Compressible Flow*. Tata McGraw-Hill Education.

Colonius, T. 2004 Modeling artificial boundary conditions for compressible flow. *Annu. Rev. Fluid Mech.* **36**, 315–345.

Colonius, T., Lele, S. K. & Moin, P. 1993 Boundary conditions for direct computation of aerodynamic sound generation. *AIAA J.* **31**, 1574–1582.

Engquist, B. & Majda, A. 1977 Absorbing boundary conditions for numerical simulation of waves. *Proc. Natl. Acad. Sci. USA* **74**, 1765–1766.

Freund, J. B. 1997 Proposed inflow/outflow boundary condition for direct computation of aerodynamic sound. *AIAA J.* **35**, 740–742.

Giles, M. B. 1990 Nonreflecting boundary conditions for Euler equation calculations. *AIAA J.* **28** (12), 2050–2058.

Gottlieb, S. & Shu, C.-W. 1998 Total variation diminishing Runge-Kutta schemes. *Math. Comput.* **67**, 73–85.

Hagstrom, T. 1999 Radiation boundary conditions for the numerical simulation of waves. *Acta Numer.* **8**, 47–106.

Jiang, G.-S. & Shu, C.-W. 1996 Efficient implementation of weighted ENO schemes. *J. Comput. Phys* **126**, 202–228.

LeVeque, R. J. 2002 *Finite Volume Methods for Hyperbolic Problems*. Cambridge University Press.

Mani, A. 2012 Analysis and optimization of numerical sponge layers as a nonreflective boundary treatment. *Journal of Computational Physics* **231** (2), 704–716.

Poinsot, T. & Lele, S. 1992 Boundary conditions for direct simulations of compressible viscous flows. *J. Comput. Phys* **101**, 104–129.

Rudy, D. H. & Strikwerda, J. C. 1980 A nonreflecting outflow boundary condition for subsonic Navier-Stokes calculations. *J. Comput. Phys* **36**, 55–70.

Thompson, K. W. 1987 Time dependent boundary conditions for hyperbolic systems. *J. Comput. Phys* **68**, 1–24.

Thompson, K. W. 1990 Time-dependent boundary conditions for hyperbolic systems, II. *J. Comput. Phys* **89**, 439–461.